Sub-wavelength nanofluidics in photonic crystal sensors

Min Huang,[1,2] Ahmet Ali Yanik,[1,2], Tsung-Yao Chang[4] and Hatice Altug[1,2,3*]

[1] *Department of Electrical and Computer Engineering, Boston University, Boston, MA, 02215, USA*
[2] *Boston University Photonics Center, Boston, MA, 02215, USA*
[3] *Division of Material Science and Engineering, Boston, MA, 02215, USA*
[4] *Department of Electrical Engineering and Computer Science, Massachusetts Institute of Technology, Cambridge, MA, 02139, USA*
**altug@bu.edu*

Abstract: We introduce a novel sensor scheme combining nano-photonics and nano-fluidics on a single platform through the use of free-standing photonic crystals. By harnessing nano-scale openings, we theoretically and experimentally demonstrate that both fluidics and light can be manipulated at sub-wavelength scales. Compared to the conventional fluidic channels, we actively steer the convective flow through the nanohole openings for effective delivery of the analytes to the sensor surface. We apply our method to detect refractive index changes in aqueous solutions. Bulk measurements indicate that active delivery of the convective flow results in better sensitivities. The sensitivity of the sensor reaches 510 nm/RIU for resonance located around 850 nm with a line-width of ~10 nm in solution. Experimental results are matched very well with numerical simulations. We also show that cross-polarization measurements can be employed to further improve the detection limit by increasing the signal-to-noise ratio.

©2009 Optical Society of America

OCIS codes: (350.4238) Nanophotonics and photonic crystals; (280.1415) Biological sensing and sensors; (050.6624) Subwavelength structures; (260.5740) Resonance; (170.0170) Medical optics and biotechnology; (220.4241) Nanostructure fabrication.

References and links

1. A. N. Shipway, E. Katz, and I. Willner, "Nanoparticle arrays on surfaces for electronic, optical, and sensor applications," ChemPhysChem **1**(1), 18–52 (2000).
2. R. Raiteria, M. Grattarola, and R. Berge, "Micromechanics senses biomolecules," Materials Today **5**(1), 22–29 (2002).
3. D. Erickson, S. Manda, and H. J. Allen, Yang and B. Cordovez, "Nanobiosensors: optofluidic, electrical and mechanical approaches to biomolecular detection at the nanoscale." Microfluid. Nanofluid. **4**(1–2), 33–52 (2007).
4. P. S. Waggoner, and H. G. Craighead, "Micro- and nanomechanical sensors for environmental, chemical, and biological detection," Lab Chip, Volume **7**(10), 1238–1255 (2007).
5. C. Monat, P. Domachuk, and B. J. Eggleton, "Integrated optofluidics: A new river of light," Nature Photon. **1**(2), 106–114 (2007).
6. B. Kuswandi, J. Nuriman, J. Huskens, and W. Verboom, "Optical sensing systems for microfluidic devices: A review," Analytica Chimica Acta **601**(2), 141–155 (2007).
7. P. E. Sheehan, and L. J. Whitman, "Detection limits for nanoscale biosensors," Nano Lett. **5**(4), 803–807 (2005).
8. J. Bishop, S. Blair, and A. Chagovetz, "Convective flow effects on DNA biosensors," Biosens. Bioelectron. **22**(9-10), 2192–2198 (2007).
9. T. M. Squires, R. J. Messinger, and S. R. Manalis, "Making it stick: convection, reaction and diffusion in surface-based biosensors," Nature Biotechnol. **26**(4), 417–426 (2008).
10. J. P. Golden, T. M. Floyd-Smith, D. R. Mott, and F. S. Ligler, "Target delivery in a microfluidic immunosensor," Biosens. Bioelectron. **22**(11 Issue 11), 2763–2767 (2007).
11. R. W. Boyd, and J. E. Heebner, "Sensitive disk resonator photonic biosensor," Applied Optics, Volume **40**(31 Issue 31), 5742–5747 (2001).

#118075 - $15.00 USD Received 21 Oct 2009; revised 9 Nov 2009; accepted 9 Nov 2009; published 18 Dec 2009
(C) 2009 OSA

12. A. J. Haes, S. Zou, G. C. Schatz, and R. P. Van Duyne, "A Nanoscale Optical Biosensor: The Long Range Distance Dependence of the Localized Surface Plasmon Resonance of Noble Metal Nanoparticles," J. Phys. Chem. B **108**(1), 109–116 (2004).
13. A. J. Haes, and R. P. Van Duyne, "A unified view of propagating and localized surface plasmon resonance biosensors." Anal. Bioanal. Chem. **379**(7–8), 920–930 (2004).
14. A. D. Leebeeck, L. K. Swaroop Kumar, V. D. Lange, D. Sinton, R. Gordon, and A. G. Brolo, "On-Chip Surface-Based Detection with Nanohole Arrays," Anal. Chem. **79**(11), 4094–4100 (2007).
15. A. Artar, A. A. Yanik, and H. Altug, "Fabry–Pérot nanocavities in multilayered plasmonic crystals for enhanced biosensing," Appl. Phy. Lett. **95**(5), 051105 (2009).
16. E. Chow, A. Grot, L. W. Mirkarimi, M. Sigalas, and G. Girolami, "Ultracompact biochemical sensor built with two-dimensional photonic crystal microcavity," Opt. Lett. **29**(10), 1093–1095 (2004).
17. H. Altug, and J. Vuckovic, "Polarization control and sensing with two-dimensional coupled photonic crystal microcavity arrays," Opt. Lett. **30**(9), 982 (2005).
18. N. Skivesen, A. Têtu, M. Kristensen, J. Kjems, L. H. Frandsen, and P. I. Borel, "Photonic-crystal waveguide biosensor," Opt. Express **15**(6), 3169–3176 (2007).
19. L. Shi, P. Pottier, Y.-A. Peter, and M. Skorobogatiy, "Guided-mode resonance photonic crystal slab sensors based on bead monolayer geometry," Opt. Express **16**(22), 17962–17971 (2008).
20. O. Levi, M. M. Lee, J. Zhang, V. Lousse, S. R. J. Brueck, S. Fan, and J. S. Harris, "Sensitivity analysis of a photonic crystal structure for index-of-refraction sensing," Proc. SPIE **6447**, 2–9 (2007).
21. D. Nedelkov, and R. W. Nelson, "Surface plasmon resonance mass spectrometry: recent progress and outlooks," Trends in Biotechnology, Volume **21**(7 Issue 7), 301–305 (2003).
22. S. Mandal, and D. Erickson, "Nanoscale optofluidic sensor arrays," Opt. Express **16**(3), 1623–1631 (2008).
23. A. M. Armani, R. P. Kulkarni, S. E. Fraser, R. C. Flagan, and K. J. Vahala, "Label-Free, Single-Molecule Detection with Optical Microcavities." Science **317**(5839), 783–787 (2007).
24. S. Chana, Y. Li, L. J. Rothberg, B. L. Miller, and P. M. Fauchet, "Nanoscale silicon microcavities for biosensing." Mat. Scie. Engin. C **15**(1–2), 277–282 (2001).
25. S. Fan, and J. D. Joannopoulos, "Analysis of guided resonances in photonic crystal slabs," Phys. Rev. B **65**(23), 235112 (2002).
26. I. D. Block, N. Ganesh, M. Lu, and B. T. Cunningham, "A sensitivity model for predicting photonic crystal biosensor performance," IEEE Sensors **8**(3), 274–280 (2008).
27. K. A. Tetz, L. Pang, and Y. Fainman, "High-resolution surface plasmon resonance sensor based on linewidth-optimized nanohole array transmittance," Opt. Lett. **31**(10), (1528–1530).

1. Introduction

In recent years, label free bio-sensors combined with innovative signal transduction methods are proposed to push the detection limits down to femto-molar concentrations of analytes [1–3]. Concurrently, researchers are integrating such sensitive and compact nano-sensors with micro-fluidics for automated sample handling [4, 5]. While micro-fluidics can enable portable and lab-on-a-chip systems, recent theoretical and numerical calculations indicate that we have to take into account the effects of various fluidic integration schemes as they can fundamentally limit the sensor performances [6]. For nano-sensors embedded in conventional microfluidic channels, the detection limit is often determined by the analyte (mass) transport limitations as opposed to the detection capabilities of the sensors [7]. As the analytes are collected by the functionalized sensors, depletion zones form around the sensing area. Depletion zone, where the analytes transport diffusively, expands with time until its growth is halted by the convective flow [8, 9]. In micro-fluidic channels supporting laminar flow profile, the convective flow parallel to the surface is weaker close to the channel edge. Accordingly, the depletion zones extend significantly towards the center of the channel. It causes dramatically lower amounts of analytes to reach the sensing surface per unit time [10]. Consequently, if no method is introduced to actively direct the convective flow towards the surface of the nano-micro size sensors, analytes at low concentrations may need week-to-years to diffuse due to mass (analyte) transport limitations imposed by the depletion zones [7].

In this paper, we introduce a novel sensing scheme which merges nano-fluidics and nano-photonics on the same platform. Within the last decade, several highly sensitive optical label-free nano-sensors have been introduced: such as dielectric resonators supporting whispering-gallery modes [11], metallic nano-structures supporting localized/propagating surface plasmons [12–15], and photonic crystals (PhC) supporting cavity [16, 17], waveguide [18] and guided resonance modes [19, 20]. Among these, nanohole array based platforms are

#118075 - $15.00 USD Received 21 Oct 2009; revised 9 Nov 2009; accepted 9 Nov 2009; published 18 Dec 2009
(C) 2009 OSA

offering more freedom to manipulate the spatial extent and the spectral characteristics of the electromagnetic fields. Furthermore, nanoholes also provide a natural platform to transport the liquid at the nano-scales: a unique opportunity that has not been explored yet. In this work, we employ suspended PhC with nano-scale openings as our sensing platform. We use their optical resonances for label-free detection. At the same time, we utilize the openings to actively steer the convective flow to the surface to overcome the mass transport limitations. We present both theoretical and experimental analysis of the fluidics and the photonic components of our integrated system. As we show below, the proposed scheme offers enhancements in the sensor performance and the sensitivity.

2. Device scheme and the flow analysis

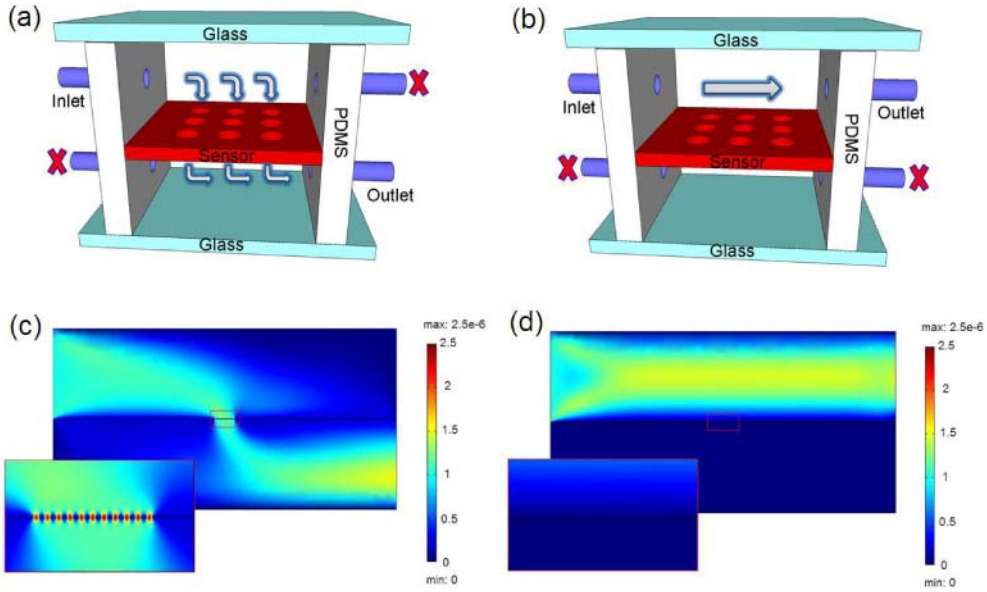

Fig. 1. (a) Illustration of the actively controlled flow scheme. Solution directed to the structure surface goes through the nano-scale hole arrays and flows to the bottom channel. The nanohole arrays are used as sensing structures as well as nanofluidic channels. (b) Conventional (passively controlled) flow scheme is illustrated. Convective flow stream passes over the surface of the sensor. (c)-(d) Velocity distribution of solutions are calculated by solving the Navier-Stokes equations for actively and passively controlled flow scheme. Insets show the distribution around the nanohole arrays in detail.

Figure 1(a) illustrates our proposed platform for active control of convective flow. The free standing PhCs are sealed in a chamber such that only the nano-scale hole arrays enable the flow between the top and the bottom channels. This is contrary to the conventional approach in which the convective flow stream passes over the sensor (Fig. 1(b)). To compare the flow profile of our proposed scheme with the conventional approach, Navier-Stokes equations are solved numerically using finite element method in COMSOL^{TM}. The simulations are done in two-dimensions using incompressible isothermal fluid flow. In the model, we use two microfluidic channels (on top and bottom) with 200 μm in length and 50 μm in height. A row of 10 rods spaced by 0.6 μm represents the nanohole arrays. The opening at the top left side of the microfluidic channel is used as the inlet to flow the solution (water) to the chamber at a velocity of 10^{-6} m/s. The openings at the bottom and the top right side with no pressure applied are used as an outlet for the actively controlled and the conventional fluidic flow schemes, respectively. The spacing between the rods is defined as continuous boundary which allows the solution to flow through, while the other boundaries are treated as no slip walls.

#118075 - $15.00 USD Received 21 Oct 2009; revised 9 Nov 2009; accepted 9 Nov 2009; published 18 Dec 2009
(C) 2009 OSA

Figure 1(c) and (d) show the steady state velocity distribution for the actively (proposed) and the passively (conventional) controlled convective flow schemes. Flow profiles around PhC regions are shown in detail (insets). For the passively controlled scheme (Fig. 1(d)), as the viscous forces in the fluid dominate over the inertial forces, we observe the formation of laminar flow profile. The convective flow is fast close to the center of the channel but becomes very slow near the edges. This implies that in an immunoassay based sensing the depletion zones will extend further from the sensor surface causing ever slower analyte transport. One can increase the convective flow rate to shrink the depletion zones. However, such a passive (indirect) control only results in moderate improvements in mass transport rates [9]. The alternative approach we propose here to overcome the mass transport limitation is to steer the convective flow directly towards the sensing surface. This is demonstrated in microfludic simulation in Fig. 1(c) where the convective flow is still very strong around the sensing surface and the turbulences (stirring of the solution) are generated around the holes. Such a directed flow can strongly improve the delivery of the analytes to the sensor surface. This scheme also helps to overcome the surface tension of highly viscous solution and guarantees that the sensor can be totally immersed in solution. In this way, as both sides of the structure are exposed to the solution, the sensitivity is further enhanced.

3. Device fabrication and sensor design

3.1 Device fabrication

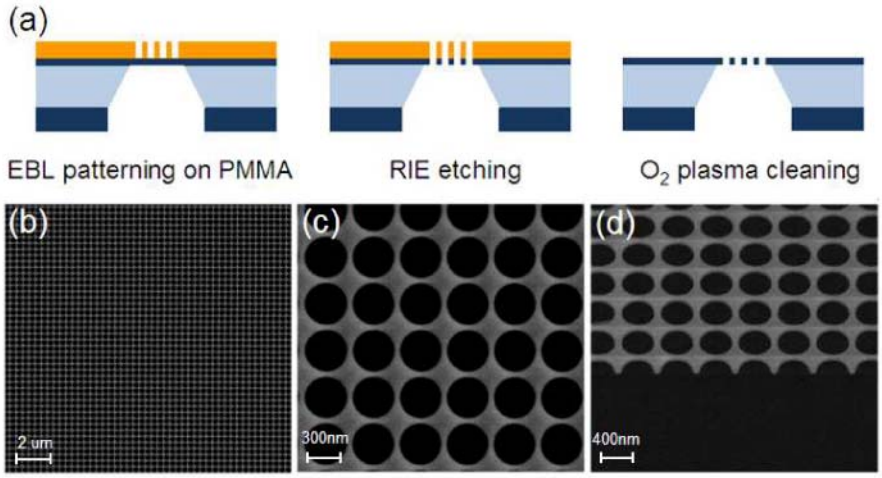

Fig. 2. (a) Fabrication scheme. Structure is first patterned on Polymethyl methacrylate (PMMA) layer using EBL. Then reactive ion etching (RIE) is used to dry etch the SiN_x slab. PMMA left on the structure is cleaned using O_2 plasma asher, resulting in a suspended PhC membrane. (b)-(c) SEM top view of the structure. (d) SEM cross-view of the structure titled at 40°.

In order to implement the proposed scheme, we use PhC structures on free standing membranes. One important consideration here is the mechanical strength of the membranes as they need to stand the relatively high pressures generated by the perpendicular convective flow. Mechanically highly robust Low Pressure Chemical Vapor Deposition (LPCVD) silicon nitride (SiN_x) films are excellent choice. In addition, LPCVD SiN_x films have very good optical properties for the implementation of PhCs. They are transparent in the visible/near-infrared regime with high refractive index. Figure 2(a) summarizes the fabrication steps. We start with ~200 x 200 μm^2 area free-standing SiN_x membranes. PhCs are fabricated by performing e-beam lithography (EBL) and dry-etching. Scanning Electron Microscopy (SEM) images of the fabricated structures are shown in Fig. 2(b), 2(c) and 2(d). The tilted SEM

#118075 - $15.00 USD Received 21 Oct 2009; revised 9 Nov 2009; accepted 9 Nov 2009; published 18 Dec 2009
(C) 2009 OSA

image taken at 40° confirms the vertical wall profiles of the openings. The thickness of the fabricated membranes (~90 nm) is much smaller compared to the membrane area (~40,000 μm^2). Although the aspect ratio is very high, the membranes are observed to survive long hours of operation under flow pressure.

3.2 Photonic crystal sensor design

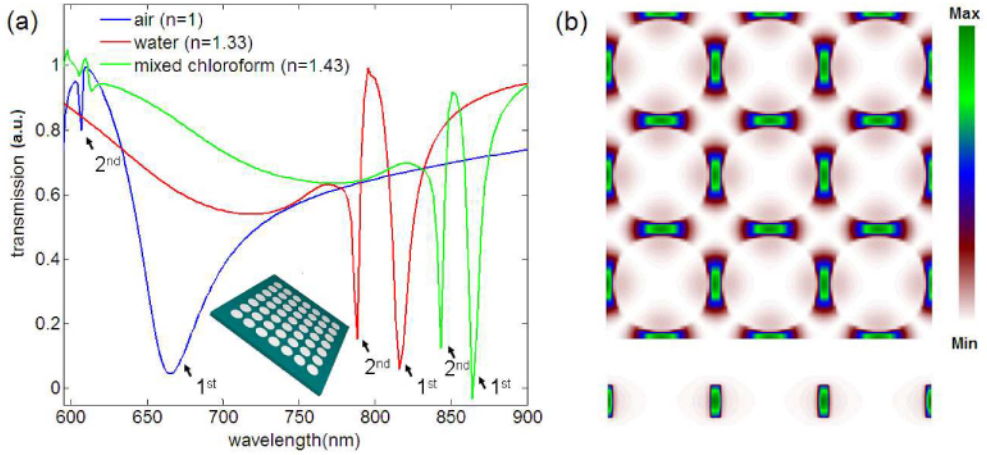

Fig. 3. PhC sensor design: (a) Transmission spectra calculated by 3D-FDTD simulations are shown when the PhC slab is emerged in three different media: air (blue), water (red) and an IPA-chloroform mixture (green), respectively. Inset shows the schematic view of the design. Parameters for the structure are: r = 270 nm, a = 600 nm and d=90nm. (b) Electromagnetic intensity distribution of the 1st mode when the structure is in air. Top and cross section views are shown, respectively.

PhCs offer unique opportunities to tailor the spatial extent of the electromagnetic field and control the strength of the light-matter interaction. In this work, we exploit guided resonances that are delocalized in the plane and tightly confined in the vertical direction. The periodic index contrast of the structures enables the excitation of the guided resonances with a plane-wave illumination at normal incidence and their out-coupling into the radiation modes. Such a surface normal operation eliminates the alignments of sensitive prism/waveguide/fiber coupling schemes needed by other optical nanosensors [21–24]. The ease of resonance excitation by surface normal light is particularly advantageous for high-throughput micro-array applications. The incident light is transmitted by PhC slabs through two different pathways [25]. One of them is the direct pathway, where a portion of the electromagnetic field goes straight through the slab. The other is the indirect pathway, where the remaining portion couples into the guided resonances before leaking into the radiation modes. These two pathways interfere with each other and result in resonances with sharp Fano-type asymmetric line-shapes. The spectral location of these resonances is highly sensitive to the refractive index changes occurring within the surroundings of PhC slabs. The index change due to the accumulation of bio-molecules or variations in the bulk solution could be detected optically in a label-free fashion.

To experimentally implement the proposed sensor, we use square lattice SiN_x PhC slabs (inset in Fig. 3(a)). Figure 3(a) shows the transmission spectra of a specific design calculated by three dimensional finite-difference time-domain (3D-FDTD) method in three different media: air (refractive index n = 1), water (n = 1.33), and an IPA-chloroform mixture (n = 1.43). A normally incident plane wave source (corresponding to the Γ-point in the dispersion diagram) excites the eigenmodes of the system. For each case, two modes are observed within the given spectral range. Figure 3(b) shows the intensity distribution of the lowest (first) order

#118075 - $15.00 USD Received 21 Oct 2009; revised 9 Nov 2009; accepted 9 Nov 2009; published 18 Dec 2009
(C) 2009 OSA

mode when the structure is in air. The field has four-fold symmetry as the lattice and well confined within the slab in the vertical direction. Within the plane, the field extends into the holes, which is crucial in increasing the field overlap with the surrounding media for higher sensitivity. We evaluate its bulk sensitivity (in units of nm/RIU) by calculating the shift of the resonance position in wavelength versus the refractive index change in the surrounding environment. To optimize the structure for higher sensitivity, we studied the effects of the slab thickness and the hole radius by varying the thickness d from 0.1a to 0.3a and the radius r from 0.3a to 0.45a (a is the periodicity). For all the analyzed structures, the resonant wavelength of the lowest order mode in air is scaled to 670 nm. The calculated sensitivities and the parameter sets for each case are given in Table 1. The sensitivity improves as the size of the holes increases and the slab thickness decreases. When r=0.45a and d=0.1a, the sensitivity reaches 560 nm/RIU. Given the difficulty of fabricating such a thin membrane, we instead use the design with thickness d=0.15a**.** Its sensitivity is still over 535 nm/RIU. As the sensitivity scales with wavelength, shifting the resonances to the longer wavelength (such as 1550 nm range) could increase the sensitivity even further (well above 1000 nm/RIU).

Table 1. Sensitivity results with different hole radius and slab thickness (in unit of nm/RIU)

d \ r	0.3a	0.35a	0.4a	0.45a
0.1a	405	485	490	560
0.15a	317	351	422	535
0.2a	236	344	370	500
0.3a	230	281	307	388

The optimized PhC structures are fabricated on free standing SiN_x membranes according to the process flow described in Fig. 2. SEM images indicate that the diameter and the periodicity are 540 nm and 605 nm, respectively. Ellipsometer measurements are taken on the unpatterned area of the membrane to confirm that the slab thickness is ~90 nm. These numbers are quite close to the optimized design with r/a=0.45 and d/a=0.15. For the PhC with periodicity of 605 nm, the resonance peak in air is located at ~670nm. This wavelength is well within the spectral coverage of our experimental setup.

4. Experimental results

4.1 Controlling the flow

To carry out the flow tests, the structures are integrated in a chamber with two inlets/outlets both on the top and the bottom channels fabricated in polydimethylsiloxane (PDMS). To implement the laminar flow scheme, where the convective flow is parallel to the surface (Fig. 1(b) and Fig. 1(d)), we blocked the inlet/outlet of the bottom channel. To steer the convective flow actively towards the sensing surface, we blocked one of the openings of the both channels (Fig. 1(a) and Fig. 1(c)). The PhC slab is sealed perfectly to ensure the flow is only through the openings. Video images of the perpendicular convective flow, captured in a microscope with a CCD camera, are shown in Fig. 4. (***video stream is available in the supplementary***). Here, the IPA solution is pumped into the bottom channel by a syringe at a rate of 80μL/s. The video recording starts when the bottom channel is almost filled-up. Figure 4 (and video) shows the merge of IPA to the top channel only through the openings, confirming the active steering of the liquid flow. No damage or breakage of the membrane due to the applied pressure is observed.

#118075 - $15.00 USD Received 21 Oct 2009; revised 9 Nov 2009; accepted 9 Nov 2009; published 18 Dec 2009
(C) 2009 OSA

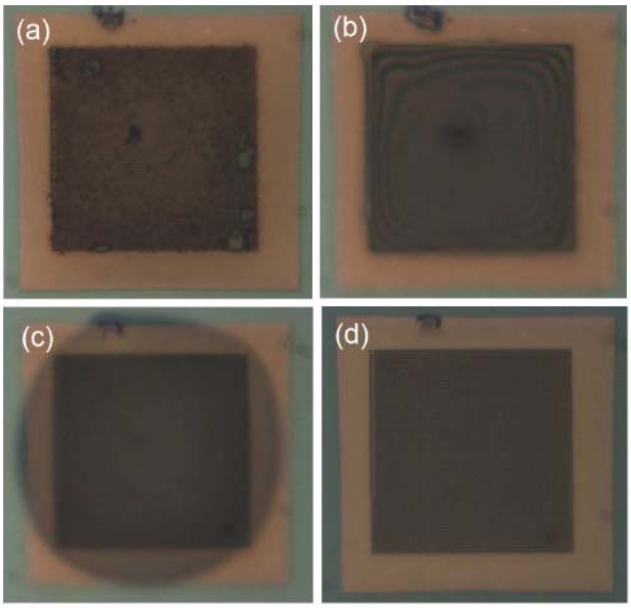

Fig. 4. (Media 1) images of the actively directed perpendicular convective flow: (a) Bottom channel is almost filled up with IPA. (b) IPA starts to go through the nanohole openings. (c) IPA spreads over the surface. (d) The whole structure is emerged in IPA.

4.2 Sensor response comparison for the actively controlled and conventional schemes

To experimentally evaluate the sensing response of the different flow schemes, transmission spectra of PhCs are obtained by launching a collimated and unpolarized light at normal incidence. The transmitted signal is collected with a 0.7 numerical aperture objective lens and coupled into a spectrometer for spectral analysis. The comparison of the transmitted spectra is shown in Fig. 5(a). Blue curve is the transmission spectrum taken in air, which clearly shows the excitation of the lowest and the next higher order modes at 667 nm and 610 nm, respectively. The red and the green curves are the responses in the solution (DI-water) for both flow schemes. When the convective flow is parallel to the surface (green curve), no leakage to the bottom surface is observed due to the large surface tension of the DI-water. On the other hand, when the convective flow is actively directed through the openings, PhC membrane is totally immersed in DI-water. This results in a larger refractive index change and more than 40 nm additional resonance shift. This observation is also confirmed by numerical simulations. 3D-FDTD calculations are performed for the PhCs in air and totally immersed in water. The slab parameters are obtained from SEM images and ellipsometer measurements. Figure 5(b) and (c) shows the simulation results overlaid directly with the experimental measurements without any shifting. Near perfect match between the resonance locations and the line-widths are observed for both modes. There is a slight distortion in the resonance shape of the first mode in air, which could be due to fabrication disorder. We also performed simulation for the case in which water fills only the top channel (such that the holes and the bottom channel are still in air). The calculated resonance position for the lowest order mode (data not shown) is nearly same with the experimental result (green curve in Fig. 5(a)). This indicates that due to the large surface tension, solutions cannot penetrate through the nanoholes if no steering method is employed. We observed both in theory and experiment that the widths of the resonance peaks are significantly narrower when the structure is immersed in solution. This is due to the reduction of the index contrast within the slab resulting in less efficient coupling with the radiation continuum. With reduced index contrast (which could be

#118075 - $15.00 USD Received 21 Oct 2009; revised 9 Nov 2009; accepted 9 Nov 2009; published 18 Dec 2009
(C) 2009 OSA

due to immersion in solution or reduction of hole size [25]), guided resonances asymptotically turns into fully confined slab modes with infinite Q factors and narrow line-widths.

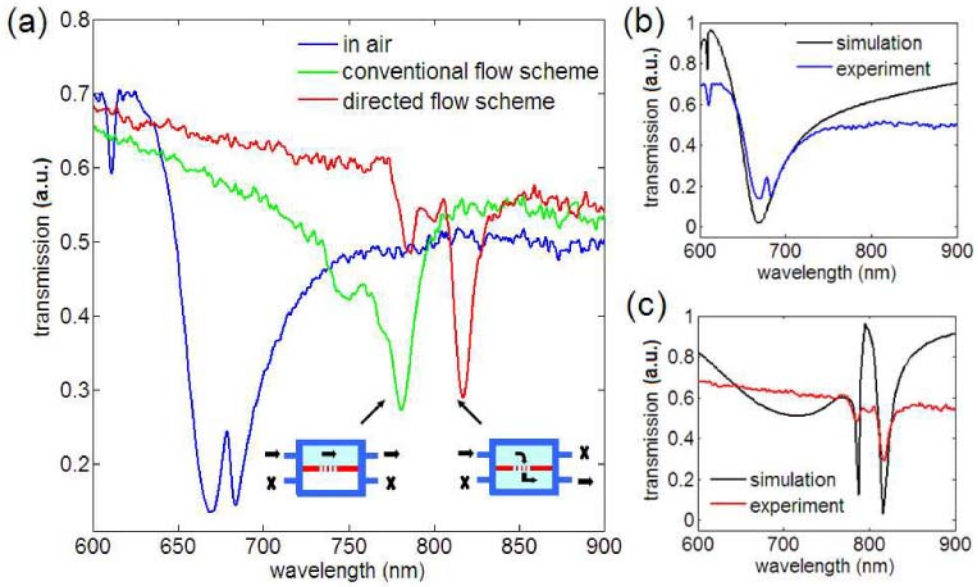

Fig. 5. (a) Experimental comparison of transmission spectra for two different flow schemes. Actively controlled flow scheme (red) shows better sensitivity and narrower linewidth compared to the conventional scheme (green). (b) Experimentally measured transmission spectrum in air (blue) is overlaid with the simulation result (black). (c) Experimentally measured transmission spectrum in water (red) is overlaid with the simulation result (black).

4.3 Sensor sensitivity for the actively controlled delivery scheme

Bulk sensitivity of the PhCs is tested by successively applying five different solutions through the directed flow scheme: DI-water, acetone, IPA and two IPA-chloroform mixtures with refractive indices of 1, 1.33, 1.356, 1.377, 1.401 and 1.424, respectively. The refractive indices of all the liquids are initially measured using a commercial refractometer. The measurements are performed by slowly pumping the solution to the chamber at 50 μL/s pumping rate. Prior to each measurement, we make sure the former solution is entirely replaced by the new one. As shown in Fig. 6(a), with increasing refractive index the resonances red-shift and the line-widths become narrower. The linewidth of the resonance in DI-water is measured to be ~10 nm. Figure 6(b) shows the shift in resonance wavelength versus the refractive index of the liquid. The agreement between the experimental data and the theoretically predicted shifts is excellent. The experimentally measured sensitivity of the sensor, 510 nm/RIU for operation near 850 nm in wavelength, is much larger than the previously reported values [20, 26].

#118075 - $15.00 USD Received 21 Oct 2009; revised 9 Nov 2009; accepted 9 Nov 2009; published 18 Dec 2009
(C) 2009 OSA

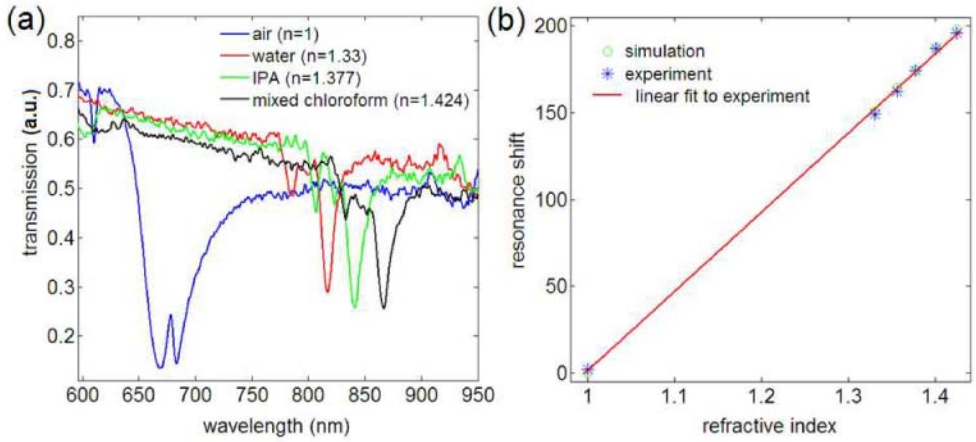

Fig. 6. (a) Experimentally measured transmission spectra of PhC slab using actively controlled delivery scheme in air (blue), water (red), IPA (green) and an IPA-chloroform mixture (black). (b) Shifts of the 1st resonant peaks in wavelength versus the surrounding refractive index. Resonance peak positions found in experiments (blue stars) match very well with the simulation results (green circles). Red line is a linear fitting to the experimental results.

4.4 Isolating the resonances with large signal-to-noise ratio

As we show above, with the demonstrated sensor system, we can effectively detect the refractive index changes by tracking the resonances. However, minute amounts of analytes from small quantities of biological samples would result in very small resonance peak shifts. In such cases, it is crucial to have narrow resonances with large signal-to-noise ratios. This can be achieved by using cross-polarization measurements [17,27]. As mentioned above, the transmission spectra result from interference of two optical paths: one is the direct transmission while the other is through the guided resonances. When we employ an unpolarized light and collect all the light transmitted through the slab, both pathways contributes to the detected signal. However, if we launch a polarized light and collect the signal after an analyzer oriented perpendicular to the polarizer, only the scattering from the guided resonances contributes. This results in dramatic suppression of the background and isolation of the resonances with large signal-to-noise ratios. In addition, the cross-polarization measurements result in purely Lorentzian-shape resonance profiles with narrower line-widths. Figure 7(a) compares the cross-polarization spectrum (red) with the regular one (blue). The spectra are taken when the structure is in air. Cross-polarization measurements clearly isolate two distinct resonance features from the background. A single Lorentzian with 7 nm line-width fits very well with the second order mode resonance (Fig. 7(b)). On the other hand, two Lorenztians are needed to fit the lowest order mode (Fig. 7(b)). This indicates a potential resonance splitting for the lowest order mode, which could be due to a slight non-uniformity in fabrication. The addition of three Lorentzians (red dashed curve in Fig. 7(b)) matches very well with the experimentally measured spectrum.

#118075 - $15.00 USD Received 21 Oct 2009; revised 9 Nov 2009; accepted 9 Nov 2009; published 18 Dec 2009
(C) 2009 OSA

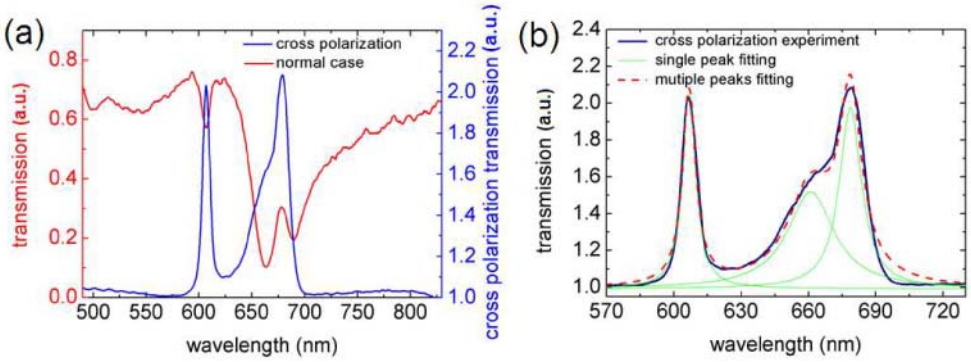

Fig. 7. (a) Cross polarization spectrum (blue) and the regular unpolarized measurement (red). (b) Green curves correspond to the fitting of the resonance feature in the spectrum with single Lorentzian functions. Their summation is denoted in red dashed line and overlaid with the experimental result (blue curve).

5. Conclusion

In conclusion, we introduced a novel sensor combining nano-photonics and nano-fluidics on a single platform. By using nano-scale openings in PhCs, we show that both light and fluidics can be manipulated on chip. We present both theoretical and experimental analysis of the fluidic and the photonic components of the integrated system. Compared to the laminar flow in conventional fluidic channels, we show that active steering of the convective flow results in the direct delivery of the stream to the nanohole openings. This can lead to enhanced analyte delivery to the sensor surface by overcoming the mass transport limitations. We apply our method to detect refractive index changes in aqueous solutions. Bulk measurements show that actively directed convective flow results in better sensitivities. Experimental results are matched very well with the simulations. The sensitivity of the sensor reaches 510 nm/RIU for resonance located around 850 nm with a line-width of ~10 nm in solution. We show that cross-polarization measurement can be employed to further improve the detection limit by increasing the signal-to-noise ratio.

Acknowledgment

Authors thank Rui Zhang for discussions. This work is supported in part by NSF SGER Award (ECSS-0849603), Massachusetts Life Science Center New Investigator Award (H.A.), Boston University Photonics Center and NSF Engineering Research Center on Smart Lighting (EEC-0812056).

#118075 - $15.00 USD Received 21 Oct 2009; revised 9 Nov 2009; accepted 9 Nov 2009; published 18 Dec 2009
(C) 2009 OSA